IEEE Access
Multidisciplinary ⋮ Rapid Review ⋮ Open Access Journal

Received 18 May 2023, accepted 15 June 2023, date of publication 21 June 2023, date of current version 29 June 2023.

Digital Object Identifier 10.1109/ACCESS.2023.3288340

RESEARCH ARTICLE

A Compact Broadband Circularly Polarized Patch Antenna Using Ladder Slots and Grounded Capacitors for MedRadio-Band Applications

DUCDUNG NGUYEN, (Graduate Student Member, IEEE), DANH MANH NGUYEN, (Graduate Student Member, IEEE), AND CHULHUN SEO, (Senior Member, IEEE)

Department of Information and Communication Convergence, Soongsil University, Seoul 06978, South Korea

Corresponding author: Ducdung Nguyen (nguyenducdung8692@gmail.com)

This work was supported by the National Research Foundation of Korea (NRF) through the Basic Science Research Program funded by the Ministry of Science and ICT under Grant NRF-2017R1A5A1015596.

ABSTRACT This paper presents a compact broadband circularly polarized (CP) implantable antenna at the Medical Device Radio communications Service (MedRadio) band (401-406 MHz). The proposed antenna is designed by utilizing the ladder structure slots along with shorting strategy on the radiating patch, and embedding the chip capacitors loading on the ground plane. The proposed antenna's performances are tested via numerical simulations in a three-layer phantom model. The prototypes are experimentally measured with minced pork as well as in muscle-mimicking gel, and the results show a good agreement. The experiment results indicated that the proposed CP antenna has a small overall size of 9.5 mm × 9.5 mm × 0.64 mm (57.76 mm^3) with a broad impedance matching of 25% from 350 MHz to 469 MHz, a realized gain of -31.2 dBi, and produces a wide axial ratio (AR) bandwidth of 30.5% (123 MHz with ranger from 337 MHz to 460 MHz). Moreover, the maximum specific absorption rate (SAR) value also complies with the IEEE standard safety requirements. To the best of our knowledge, the proposed CP antenna is the compactest dimension with wider impedance matching, and greater gain value (without using superstrate) and obtain CP with widest AR bandwidth compared to previously reported works in the MedRadio band.

INDEX TERMS Axial ratio, broadband, circularly polarized, implantable antenna, MedRadio.

I. INTRODUCTION

In recent years, biomedical implantable devices (IDMs) [1] have been helpful in enhancing and monitoring the patient's daily living situation and are essential in both the medical and industrial. There are various common examples of IDMs, including retinal prostheses [2], real-time glucose monitoring [3], and brain implant technologies [4], etc. An implanted antenna is a crucial and important part of IDMs that enables communication with external monitoring devices. Several frequencies have received the Federal Communications Commission (FCC) approval for using in medical applications, including Medical DeviceRadio communication Service (MedRadio, 401-406 MHz), Industrial Scientific Medical (ISM) (433-434.8 MHz; 886-906 MHz; 2.4-2.48 GHz; 5.725-5.875 GHz), and Wireless Medical Telemetry Service (WMTS 1395-1400 MHz). Among these bands, the MedRadio band attracts particular attention due to its special features designed for IMDs, such as feasibility with low power, low cost, and high data rate transmissions [5]. Due to the aforementioned issues, a number of antennas for implantable medical devices for the MedRadio band has been reported [6], [7], [8].

In terms of implanted antenna design criteria, the total dimension reduction and circular polarization (CP) are the most extensive issue need to be resolved. With miniaturization the unpleasantness to the patients will be decrease, and with CP characteristic of the antenna the communication

The associate editor coordinating the review of this manuscript and approving it for publication was Pavlos I. Lazaridis.

quality, the mobility, the efficiency and the bit-error-rates can be improved. In [9], the authors presented an antenna model that is perfectly in accordance with the design criteria of IDMs. Although the MedRadio band draws particular attentions, many studies mainly focus on miniaturizing the implantable antenna volume but very few papers are presented that address the CP issue. In addition, with the antennas which working at lower frequencies, the CP property need to be appreciated to ensure the communication link. There have been some suggested techniques for miniaturizing MedRadio band antennas such as, high-permittivity substrate [10], shorting strategy [11], meander line structure [8], embedded slots [12], capacitively loaded [13], or employed metamaterial [3]. On the other hand, the implantable antennas require a wide impedance bandwidth to prevent the frequency shift brought on by electrical characteristic of human tissue and manufacturing errors. To broaden the antenna impedance bandwidth, many methods are proposed. In [14], a flexible loop antenna with three complementary split ring resonators is utilized. In [15], a compact circularly polarized implanted antenna is introduced specifically for medical applications. The antenna demonstrates a remarkable impedance matching with the radiating patch is circular in shape and the ground plane incorporated an X-shaped slit. Other methods, such as loop antenna [16], dipole [17], have been used to improve the implantable bandwidth.

In this letter, a compact broadband implantable antenna with circular polarization at the band of 403 MHz for MedRadio band applications is presented. The proposed implantable antenna has a lowprofile of 57.76 mm^3 ($0.012\lambda \times 0.012\lambda \times 0.00085\lambda$, where λ is free-space wavelength at 403 MHz), with broad impedance matching of 25% and a wide axial ratio (AR) bandwidth of 30.5%, which attains by employing a shorting pin, etching ladder cut slots on the radiator, and embedding chip capacitors into rectangle slots in the ground plane. To validate the numerical simulation results, the designed antenna is fabricated and tested with minced pork and the muscle-mimicking gel. The simulation results and experimental testing of prototype antennas indicate good agreement. In addition, the specific absorption rate (SAR) is investigated using the CST voxel human chest model and the simulated results reveal that the SAR value compliant with IEEE standards for the safety concern. Generally, our approach exhibits exceptional qualities in comparison to previous studies, offering numerous potential applications for biomedical implantable systems in the MedRadio bands.

II. ANTENNA STRUCTURE DESIGN

A. LAYOUT OF THE PROPOSED ANTENNA

The precise geometry of the suggested antenna structure is shown in Fig. 1. The overall dimension is 9.5 mm × 9.5 mm × 0.64 mm (57.76 mm^3). Fig 1(a) shows the radiating patch, which is composed of a slot patch, a square split-ring with ladder structure, and connection pad is added between two elements. For miniaturization, a shorting pin directly

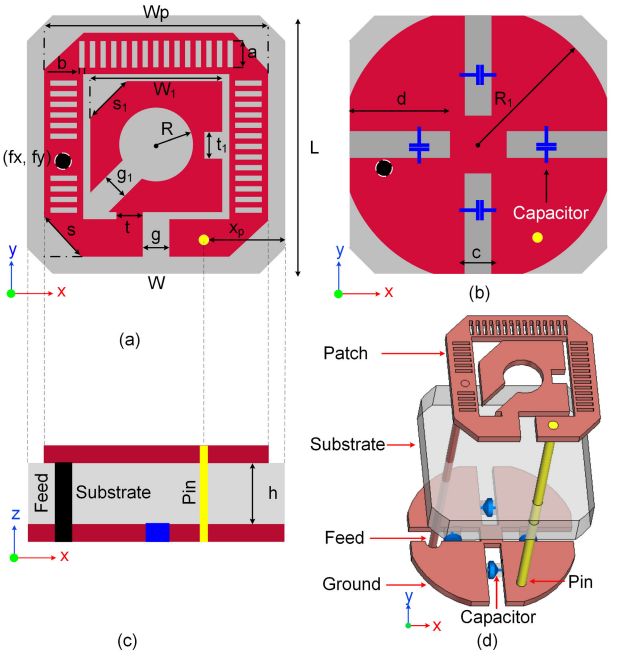

FIGURE 1. Geometry of the proposed ultra-miniaturized antenna: (a) top view, (b) back view, (c) side view, and (d) isometric view.

TABLE 1. Parameters of the designed antenna.

Par.	Value (mm)	Par.	Value (mm)	Par.	Value (mm)
W, L	9.5	R	0.98	a	1
R_1	5.1	g	1	b	0.2
W_p	8.5	g_1	1.12	c	1
W_1	5.1	t	1.05	d	4.2
x_p	2.95	t_1	1.02	fx	3.5
s	2.2	s_1	2.15	fy	0.25

connects the outer ring element to the ground plane. Fig 1(b) shows the ground plane consist of two pairs of a rectangle cut slots and four low capacitance chip capacitors ($C = 0.5pF$). Besides, the ground layer of the antenna is cut in such a way that generate four flower petals. The thickness of the ground plane is a little bit increased by reason of the real width of soldered chip capacitor (0.45mm). However, this issue does not have much impact because in practical usability the antenna will be placed inside a sealed device. With a dielectric constant of $\varepsilon_r = 10.2$, a loss tangent of $\sigma = 0.0035$, Taconic CER-10 with thickness of h = 0.64 mm is used as the substrate to provide biocompatibility. The substrate is also truncated four corners to obtain better impedance matching. In addition, the comprehensive details of the antenna are presented in Fig. 1(c), (d) with the side view and isometric view, respectively. After thorough optimization, all dimensions of the antenna are chosen, and a comprehensive summary of the designed antenna's detailed parameters can be found in Table 1.

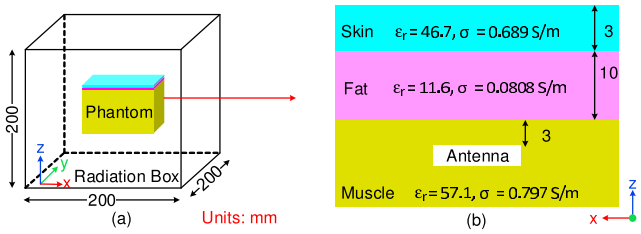

FIGURE 2. Simulation environment with multilayer tissue.

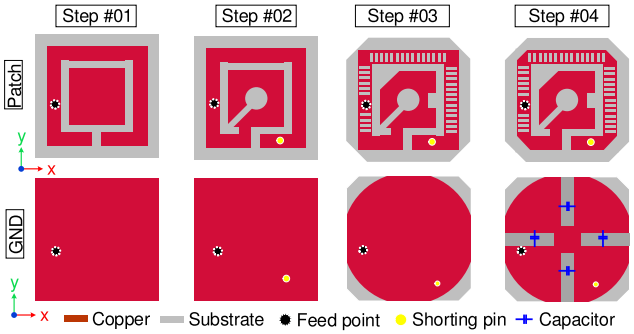

FIGURE 3. Designing steps of proposed antenna.

The proposed antenna is designed and evaluated in a three-layer phantom model containing skin, fat, and muscle with different thickness and electric characteristics at 403 MHz, as shown in Fig. 2(a). The whole size of phantom model is $90 \times 90 \times 35$ mm^3, and the antenna is placed in the muscle tissue layer with the distance of 16 mm away from the air. The dielectric permittivity (ε_r) and the conductivity (σ) of each layer at 403 MHz are exhibited in Fig. 2(b)

B. DESIGN PROCEDURE AND EQUIVALENT CIRCUIT MODEL

The suggested antenna is designed and evolved in four steps as illustrated in Fig. 3. In fact, there are several stages involved in order to obtain the latter antenna structure, however, those steps are combined to form the four main design steps. Initially, the antenna with full ground plane, a split-ring element and a square patch are utilized. Second, configuration in this step is constructed by employing a shorting pin that connects split-ring to ground plane in a proper position, adding the slots in the square patch, and a metallic pad for relating the split-ring to the patch. Then, the ladder slots on the split-ring element as well as adding corners truncated on the substrate are introduced (the implementation of truncated corners is not only utilized to avoid injuries to the human body but also contribute to improve the matching impedance). It should be emphasized that except for the bottom part the ladder structure slots are inserted around the patch periphery because the effect of the ladder slots on the stub and shorting pin will change the matching impedance of the antenna. The ground plane in the third step has four cut-off corners and is nearly circular in shape. Finally, the proposed implantable antenna with compact broadband circularly polarized at

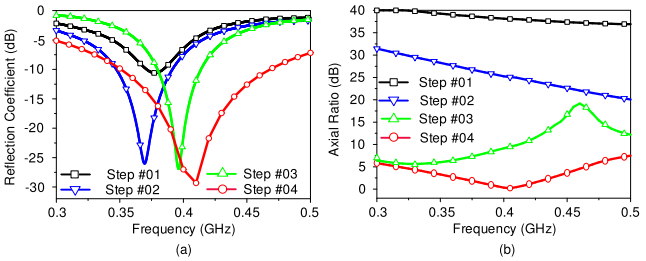

FIGURE 4. Comparison of (a) S_{11}, and (b) AR for four steps to achieve latter structure.

desired band of 403 MHz is obtained by etching the rectangle slots and embedding of the chip capacitors on the ground plane as well as truncated four corners on the patch. In this step, the ground plane is cut in such a way that generate four flower petals and the capacitors is soldered in two edges of the slots. It is worthy note that, the final step which is combination of the embedding two pairs of a rectangle cut slot and adding four low capacitance chip capacitors in one designing step.

The corresponding reflection coefficients (S_{11}) and AR values comparison of difference design steps are shown in Fig. 4. It is evident that the performance and profile of the designed implantable antenna are attained and improved enhanced step-wise. In the first step, the design starts with a large dimension of 14 mm $\times$ 14 mm $\times$ 0.64 mm, with a poor matching impedance ($S_{11} > -9.5$ dB) at the frequency operation centered 380 MHz. In the second step, the resonance frequency shifts from 380 MHz to 368 MHz (because the effect of adding shorting pin will increase the electrical length, thereby shifting the operating frequency to the lower) and the overall antenna size reduce to 12.5 mm $\times$ 12.5 mm $\times$ 0.64 mm. Then, the antenna dimension further scaled down to 9.5 mm $\times$ 9.5 mm $\times$ 0.64 mm, compare to the initial antenna dimension, the optimized structure has a size reduction of 147.3%. Herein, a shift toward higher frequency of the antenna operating resonance from 368 MHz to 398 MHz is presented after applying the third step. This issue is understandable because, by adding suitable slots on the radiator of a patch antenna can decrease the capacitance of the antenna. The capacitance of the patch with the slots is primarily determined by specific shape, size and placement of the slot. In addition, with the suitable slots on the radiator, the effective electrical length of the patch is shortened, and the surface area of the patch is reduced, which can shift the resonant frequency of the antenna to a higher frequency. The producing of the ladder structure mainly contributes for the impedance matching of proposed antenna. In the final step, the antenna resonant frequency operates exactly at 403 MHz with a broad impedance matching of 29.2% and achieved CP with a wide AR bandwidth of 34%.

When design an antenna, the extracting the equivalent circuit of a patch antenna can help in designing, optimizing, and analyzing the performance of the antenna in a circuit. In addition, the proposed antenna utilizes four low capacitance chip

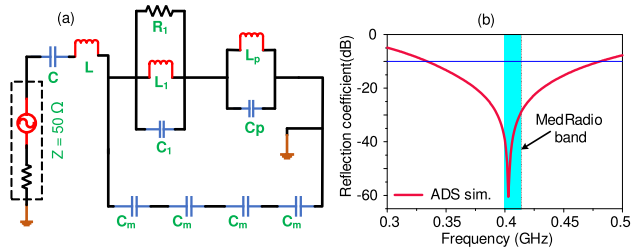

L	24.45	L_p	1.316	C	6.225	C_m	0.5
L_1	7.5	R_1	49.5	C_1	20.325	C_p	0.754

Parameters values – Unit = Ω, nH, pF

FIGURE 5. (a) Equivalent circuit and (b) Simulated S-parameter in ADS.

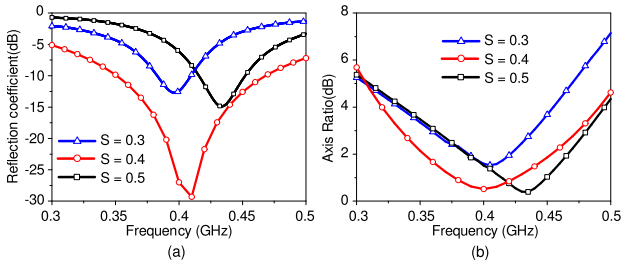

FIGURE 6. Effect of the ladder slots spacing on (a) S_{11} and (b) *AR* value.

capacitors which are soldered on the ground plane, thus, it is necessary to analysis the effect of the capacitors to the total antenna equivalent capacitance with equivalent circuit. The advanced design system (ADS) is used to create the equivalent electrical circuit model of the proposed antenna, shown in Fig. 5. Here, the resonance band is presented by using parallel-connected RLC lumped elements. The component R_1, C_1 and L_1 control the impedance matching of the operating frequency resonance. The shorting-pin is corresponding to parallel L_p and R_p. The C_m capacitors represent the embedded chip capacitors, while the capacitance and inductance are presented for C and L, respectively. Fig. 4(b) displays the S-parameter of the circuit model with the corresponding element values in ADS simulation analysis. The values of the electrical components used in the equivalent circuit are indicated in the table displayed in Fig. 5.

C. PARAMETRIC STUDY AND CIRCULAR POLARIZATION REALIZATION

This section provides comprehensive parametric analysis based on crucial design factors including the ladder slots spacing (S) and the value of chip capacitor C_m. Other parameters are not investigated in this study, thus they are not the main focus and vary depending on the mentioned variables. Furthermore, all dimensions have been optimized for the compact volume and obtaining of highest performance. The ladder structure slot represents for the compactness and the combination of rectangle slots with chip capacitors on ground plane for broadband circular polarization antenna. Therefore, the ladder structure's spacing (S) and the chip capacitor C_m value are both critical parameters in this design. It is noted that, the parametric study on the value of the chip capacitor C_m is selected based on the real value of the manufactured chip capacitor in practice, and the spacing S is calculated to avoid the overlap of the ladder form.

The parametric studies are established with identical phantom configurations to comprehend how they affect the reflection coefficient and the AR value of the designed antenna. Fig. 6 shows the impact to the simulated S_{11} and AR values of the variation with the spacing of the ladder structure on the split-ring. The value of the spacing S is varied from 0.3 mm to 0.5 mm. It is evident that the S value has an effect on the impedance matching and AR value of the antenna. The lower operating frequency band can be accomplished with smaller value of S, and vice versa. The AR value also follows this tendency. However, with different values of the ladder spacing the S_{11} depth and the AR quality gradually decrease. Thus, a value of S = 0.4 mm is chosen for good impedance matching, AR quality and closed to the desired resonant frequency.

In addition, to realize CP characteristics or enhance the antenna bandwidth, many techniques have been developed, such as, introducing a truncated patch [18], employing metamaterial. Besides these, defected ground structure (DGS) is an useful method for obtaining CP characteristic, greater Q factor, and obtain wide bandwidth [19]. Moreover, it has been found that by optimizing a suitable capacitance the antenna operating frequency and the bandwidth are not only be enhanced but also can realize the circular polarization characteristic. A 7.9 pF capacitor is introduced for increasing the equivalent element capacitor to decrease the resonance frequency [20]. In this work, the integration of four rectangle slots on the ground plane and four chip capacitors is produced to achieve the CP and enhance characteristics of proposed antenna. The two pairs of rectangles cut slot on the ground plane disrupt the uniformity of its current flow, resulting in different phases for the currents in the two orthogonal directions. Furthermore, by adjusting the capacitance in the ground plane using capacitors, the capacitance between the ground plane and the patch is altered, which in turn circular polarization can be obtained and enhanced. In this work, the grounded capacitance can be lowered or increased by forming a wider or narrower the rectangle slots width, thereby improving the total equivalent capacitance of the antenna. Nevertheless, when the dimensions of the rectangle slots are adjusted, the CP properties can change and even dissipate. To prevent this, the chip capacitors are integrated into the rectangle slots in order to modify the antenna capacitance value. Fig. 7 shows the comparison of the S_{11} and AR value based on the variation of chip capacitor values. A shift of antenna operating frequency to higher band is pointed out by using low chip capacitor value (with the conductor parts, the electrical length of the antenna increase, thus, shift the operating frequency to lower) and vice versa for higher capacitance value. However,

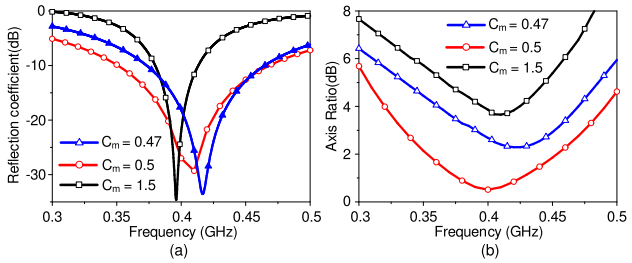

FIGURE 7. Effect of the value of capacitor on (a) S_{11} and (b) *AR* value.

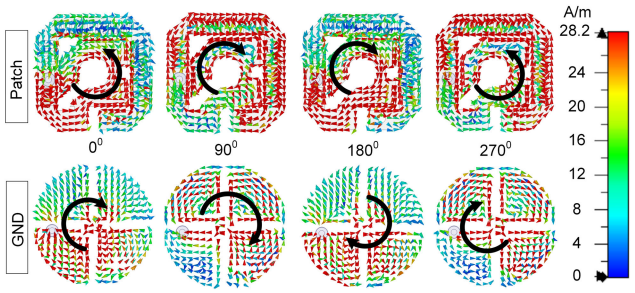

FIGURE 8. Current distribution on radiation Patch and GND at different phase of 0°, 90°, 180°, and 270°.

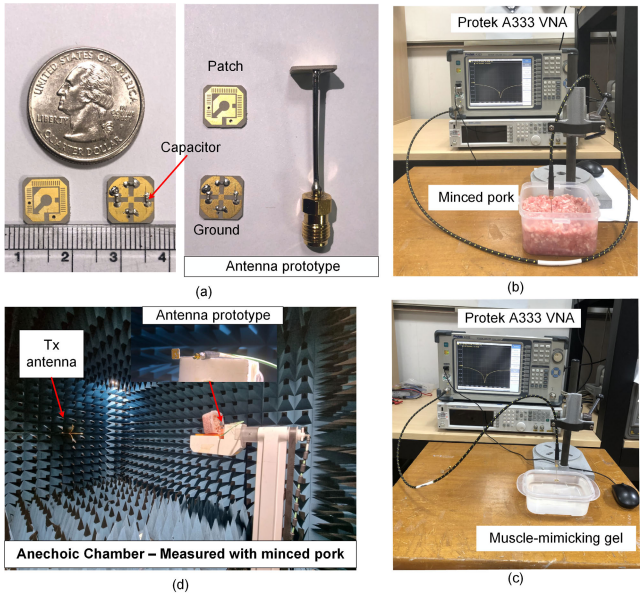

FIGURE 9. Measurement setup with (a); Fabricated prototypes. (b), (c) minced pork and muscle mimicking-gel S11 testing; and (d) radiation patterns.

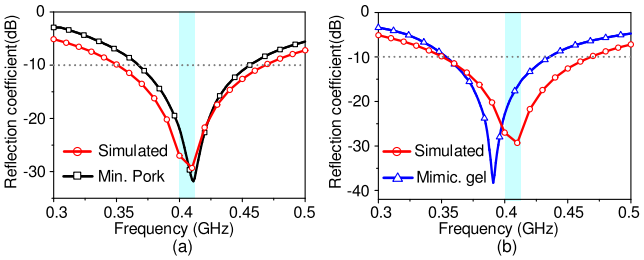

FIGURE 10. Comparison simulated and measured S-parameters results in the environment of: (a) minced-pork, (b) muscle mimicking-gel.

the embedding chip capacitor to tune the operating frequency is not purpose in this stage. In this process, by combining with the rectangle slots the the value of adoption capacitors play a significant effect on the achievement and the quality of the AR. The AR value is close to 0 dB with optimal C_m. By adopting the optimal value of $C_m = 0.5$, the antenna offers a wide impedance matching of 29.2% (350 MHz to 469 MHz) and achieves CP with wide AR bandwidth of 34%. To fully depict the CP operation mechanism of the suggested antenna, the surface current at 403 MHz for the phases of 0^0, 90^0, 180^0, and 270^0 is shown in Fig. 8. When the exited phase is 0^0 and 180^0 the stronger current concentrate at the feed and inner part of the radiation patch. When the exited phase is 90^0 and 270^0, the current distribution at the split ring with ladder slots is stronger, and also, observes two orthogonal field with the different phase of 90^0. Similarly, on the ground plane, the stronger surface current concentrates at the feed point and the petals periphery. From the figure, it is evident that the predominant surface current rotates in a clockwise, demonstrating the characteristic of left-handed circular polarization (LHCP).

III. MEASUREMENT RESULTS AND DISCUSSION

In order to validate the results achieved from the simulation scenarios, the prototypes of the designed antenna are fabricated and depicted in Fig. 9(a). The Musashi MS-1 solder machine is utilized to solder the chip capacitors and SMA coaxial cable of the fabricated antenna. Then, the characteristics of the antenna prototype are experimentally tested. The $|S_{11}|$ of the prototype for both mince pork and muscle-mimicking gel is experimentally measured through the Protek A333 vector network analyzer (VNA) with covering frequency of 300 kHz to 3.2 GHz, as illustrated in Fig. 9(b), (c). Herein, the muscle-mimicking gel is the result of mixing substances together that are Deionized Water (52.4%), Sugar (45%), and NaCl (1.4%) [21]. The comparison between simulate and measured S_{11} result of the proposed antenna in the case of mince-pork and muscle-mimicking gel are exhibited in Fig. 10. It is clearly realized that the measured result in minced pork provides the measured bandwidth ranger from 364 MHz to 463 MHz (25%), and in muscle-mimicking gel the measured bandwidth is observed to be from 352 MHz to 443 MHz (22.5%), whereas the $|S_{11}|$ below -10 dB is obtained 29.2% from 350 MHz to 469 MHz with simulation testing. Although the resonance frequencies shift slightly toward left in muscle-mimicking gel case and toward right in minced pork, the S_{11} shows a good matching impedance and the broadband can be verified. The slight different observed in the muscle-mimicking gel scenario can be attributed to the discrepancy between the

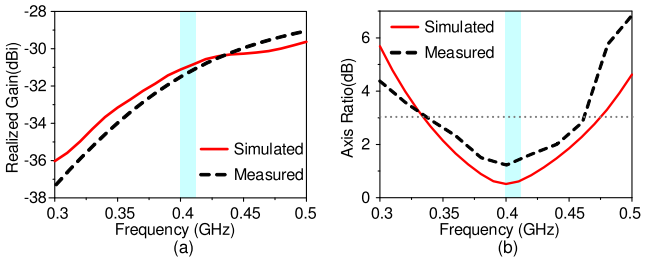

FIGURE 11. Comparison simulated and measured results of: (a) realized gain, (b) Axial ratio.

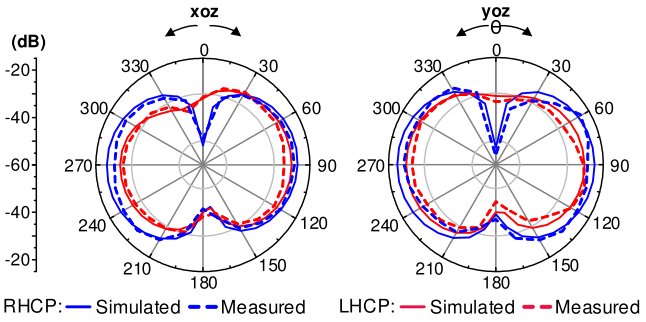

FIGURE 12. Simulation and measurement radiation pattern at 403 MHz in $x-z$ and $y-z$ planes.

dielectric properties of the measured samples and those used in the simulation [22].

Furthermore, Fig. 9(d) shows the measurement set up for gain, AR value and radiation pattern in the microwave anechoic chamber with mince-pork. The antenna system is allocated in the far-field of the transmitting antenna environment and mounted on a positioned that can be rotated freely. For measuring the radiation pattern, the prototype antenna with minced-pork box is positioned in the far-field region of the transmitting antenna, and affixed to a freely rotatable platform. In order to evaluate the radiation pattern as a function of angle, the prototype undergoes controlled rotation, enabling the transmitting antenna to illuminate the prototype from diverse angles. The measurements are taken at specific angles of 10^0, 15^0 and 30^0. Then, some undesirable points that may have resulted from connections or stacking are eliminated during the plotting process to make the graphs more smooth, and visually. Fig. 11 (a) depicts the comparison of the simulated and measured the realized gain of the proposed antenna inside minced pork. A good agreement between simulated and measured plot can be obtained and the gain value is -31.2 dBi at center frequency. In addition, Fig. 11(b) shows the simulated and the measured of $<$ 3 dB AR value of the desiged antenna at 0^0. It is clearly realized that the AR value is close to 0 dB at the center frequency, and the measured of $<$ 3 dB AR is observed from 337 MHz to 460 MHz with relative bandwidth of 30.5%, whereas obtained 34% with ranger from 335 MHz to 475 MHz in the simulation scenario, respectively. Compared to the simulation, the measured AR value and the gain shift a little to lower frequency, but could covers MedRadio band and realizes wide AR bandwidth of 123 MHz.

The radiation patterns for x-z and y-z planes are illustrated in Fig. 12. The radiation pattern of a patch antenna depends on various factors such as the shape and size of the patch and ground plane, the feed location, and the using of substrate material. From the Figure, it can be observed that the proposed antenna has a bidirectional radiation, which is result of the specific structure in this study. Furthermore, in the case of CP antenna designing, with an AR value at center frequency is lower than 1 dB, which corresponds to a 20 dB difference between LHCP and RHCP radiation patterns in both x-z and y-z planes. From the figure, it can be observed that with

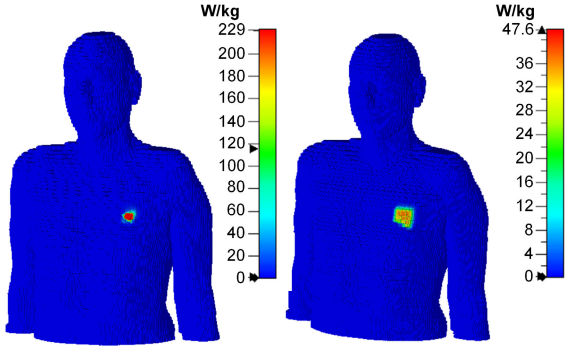

FIGURE 13. The simulation average SAR distribution for 1-g and 10-g in chest of voxel model at 403 MHz.

regardless of the simulation and measurement the radiation pattern in both x-z and y-z plane satisfies the mentioned condition. The proposed antenna shows a LHCP gain value greater than cross-polarized RHCP with values are 21 dB in the x-z plane and 22 dB in the y-z at the angle of 0^0, respectively. In addition, the antenna is evaluated averaged specific absorption rate (SAR) for consideration of human body safety. The SAR values must be in accordance with IEEE C95.1-1999 (US standard), with the peak average SAR value for 1 g of tissue limited to 1.6 W/kg and 10 g of tissue limited to 2 W/kg, respectively. In this study, the evaluation of the SAR is numerically analyzed by using the CST software with 3D voxel human chest. Fig. 13 demonstrates the SAR distribution in the chest model of the human body. Under the premise of 1 W input power, the maximum SAR of $229 W/kg$ and 47.6 W/kg with a allowed input power of $6.98 mW$ and $42.1 mW$ are realized for 1-g and 10-g IEEE standard, respectively. Finally, Table 2 compares the proposed antenna to earlier studies on implantable antennas at the MedRadio band. To best of our knowledge, there are not many publications about achieving circular polarization in the frequency range of MedRadio band. In [18] an axial ratio bandwidth of 17.82 % is achieved at 403 MHz, but with the fundamental technique of truncating patch antenna. Furthermore, in [10] an relatively broad bandwidth of 23.5 % is provided, but it has high volume with 248.92 mm^3. As can be seen, the suggested CP implabtable antenna outperform

TABLE 2. Comparison of the proposed design to state-of-art.

Ref.	Year	Freq. (MHz)	Antenna Type	Volume (mm3)	Bandwidth (%)	Gain (dBi)	SAR (1-g)	Circular Polarization	Axial Ratio (%)
[5]	2015	403	Meander Ring	198.4	7.26	-32.94	192.59	No	
[10]	2020	403	CSR	248.92	23.5	-46	338	No	
[11]	2021	403	PIFA	479	12.9	-34.9	284.5	No	-
[8]	2019	403	Meander Line	213.36	2.2	-38	-	No	-
[18]	2021	403	Truncated Patch	-	39.89	-	-	Yes	17.82
This work		**403**	**Slot Patch**	**57.76**	**25**	**-31.2**	**229**	**Yes**	**30.5**

the other reports with compactest volume, broader matching impedance, lower SAR value, higher gain (without using the superstrate) and archived CP with widest AR bandwidth.

IV. CONCLUSION

In this paper, a compact broadband implantable antenna with circular polarization in the band of 403 MHz for MedRadio band applications is proposed. The compact volume of 57.76 mm^3 ($0.012\lambda \times 0.012\lambda \times 0.00085\lambda$) is achieved through the use of a shorting pin, etching ladder cut slots on the radiator, and the embedding of chip capacitors into rectangle slots in the ground plane.A prototype is fabricated and measured via minced pork and muscle mimicking-gel to verify the simulation results. The measured results produce a broad impedance matching of 25%, a peak realized gain of -31.2 dBi, and circular polarization with a wide Axial Ratio bandwidth of 30.5%. In comparison with simulation scenario, the experimental results agree well with the simulation results. Furthermore, the SAR is also investigated using CST voxel human chest model, and the proposed antenna offers a SAR value that complies with IEEE C95.1-1999 safety guidelines. With the superior properties of the designed antenna compare to previous reports offering numerous potential applications in the MedRadio band for biomedical implantable devices. In summary, the proposed CP antenna demonstrates advantages in terms of both compact size and broad AR bandwidth.

REFERENCES

[1] W. Greatbatch and C. F. Homes, "History of implantable devices," *IEEE Eng. Med. Biol. Mag.*, vol. 10, no. 3, pp. 38–41, Sep. 1991.

[2] K. Gosalia, G. Lazzi, and M. Humayun, "Investigation of a microwave data telemetry link for a retinal prosthesis," *IEEE Trans. Microw. Theory Techn.*, vol. 52, no. 8, pp. 1925–1933, Aug. 2004.

[3] X. Y. Liu, Z. T. Wu, Y. Fan, and E. M. Tentzeris, "A miniaturized CSRR loaded wide-beamwidth circularly polarized implantable antenna for subcutaneous real-time glucose monitoring," *IEEE Antennas Wireless Propag. Lett.*, vol. 16, pp. 577–580, 2017.

[4] W. Chen, C. W. L. Lee, A. Kiourti, and J. L. Volakis, "A multi-channel passive brain implant for wireless neuropotential monitoring," *IEEE J. Electromagn., RF Microw. Med. Biol.*, vol. 2, no. 4, pp. 262–269, Dec. 2018.

[5] H. Li, Y. Guo, C. Liu, S. Xiao, and L. Li, "A miniature-implantable antenna for MedRadio-band biomedical telemetry," *IEEE Antennas Wireless Propag. Lett.*, vol. 14, pp. 1176–1179, 2015.

[6] N. Ganeshwaran, J. K. Jeyaprakash, M. G. N. Alsath, and V. Sathyanarayanan, "Design of a dual-band circular implantable antenna for biomedical applications," *IEEE Antennas Wireless Propag. Lett.*, vol. 19, no. 1, pp. 119–123, Jan. 2020.

[7] M. Yousaf, I. B. Mabrouk, F. Faisal, M. Zada, Z. Bashir, A. Akram, M. Nedil, and H. Yoo, "Compacted conformal implantable antenna with multitasking capabilities for ingestible capsule endoscope," *IEEE Access*, vol. 8, pp. 157617–157627, 2020.

[8] R. Li, B. Li, G. Du, X. Sun, and H. Sun, "A compact broadband antenna with dual-resonance for implantable devices," *Micromachines*, vol. 10, no. 1, p. 59, Jan. 2019.

[9] D. Nguyen and C. Seo, "An ultra-miniaturized circular polarized implantable antenna with gain enhancement by using DGS and holey superstrate for biomedical applications," *IEEE Access*, vol. 11, pp. 16466–16473, 2023.

[10] M. Cetindere and B. Basaran, "Compact implantable antenna design for MICS and ISM band biotelemetry applications," *Microw. Opt. Technol. Lett.*, vol. 62, pp. 1581–1587, Apr. 2020.

[11] S. Kawdungta, A. Boonpoonga, and C. Phongcharoenpanich, "MICS/ISM meander-line microstrip antenna encapsulated in oblong-shaped pod for gastrointestinal tract diagnosis," *Sensors*, vol. 21, no. 11, p. 3897, Jun. 2021.

[12] R. Li and S. Xiao, "Compact slotted semi-circular antenna for implantable medical devices," *Electron. Lett.*, vol. 50, no. 23, pp. 1675–1677, Nov. 2014.

[13] C. Liu, Y. Guo, and S. Xiao, "Capacitively loaded circularly polarized implantable patch antenna for ISM band biomedical applications," *IEEE Trans. Antennas Propag.*, vol. 62, no. 5, pp. 2407–2417, May 2014.

[14] R. S. Alrawashdeh, Y. Huang, M. Kod, and A. A. B. Sajak, "A broadband flexible implantable loop antenna with complementary split ring resonators," *IEEE Antennas Wireless Propag. Lett.*, vol. 14, pp. 1506–1509, 2015.

[15] L. Luo, B. Hu, J. Wu, T. Yan, and L. Xu, "Compact dual-band antenna with slotted ground for implantable applications," *Microw. Opt. Technol. Lett.*, vol. 61, no. 5, pp. 1314–1319, May 2019.

[16] Z. Jiang, Z. Wang, M. Leach, E. G. Lim, J. Wang, R. Pei, and Y. Huang, "Wideband loop antenna with split-ring resonators for wireless medical telemetry," *IEEE Antennas Wireless Propag. Lett.*, vol. 18, no. 7, pp. 1415–1419, Jul. 2019.

[17] S. Bakogianni and S. Koulouridis, "On the design of miniature MedRadio implantable antennas," *IEEE Trans. Antennas Propag.*, vol. 65, no. 7, pp. 3447–3455, Jul. 2017.

[18] A. Lamkaddem, A. E. Yousfi, L. E. G. Muñoz, and D. Segovia-Vargas, "A compact wideband circularly polarized implantable antenna for cardiac pacemaker devices," in *Proc. Int. Conf. Electromagn. Adv. Appl. (ICEAA)*, Aug. 2021, pp. 379–382.
[19] D. Nguyen and C. Seo, "An ultra-miniaturized antenna using loading circuit method for medical implant applications," *IEEE Access*, vol. 9, pp. 111890–111898, 2021.
[20] J. Wang, E. G. Lim, M. P. Leach, Z. Wang, R. Pei, Z. Jiang, and Y. Huang, "A 403 MHz wireless power transfer system with tuned split-ring loops for implantable medical devices," *IEEE Trans. Antennas Propag.*, vol. 70, no. 2, pp. 1355–1366, Feb. 2022.
[21] Y. Feng, Y. Li, L. Li, B. Ma, H. Hao, and L. Li, "Tissue-dependent co-matching method for dual-mode antenna in implantable neurostimulators," *IEEE Trans. Antennas Propag.*, vol. 67, no. 8, pp. 5253–5264, Aug. 2019.
[22] Z. Xia, H. Li, Z. Lee, S. Xiao, W. Shao, X. Ding, and X. Yang, "A wideband circularly polarized implantable patch antenna for ISM band biomedical applications," *IEEE Trans. Antennas Propag.*, vol. 68, no. 3, pp. 2399–2404, Mar. 2020.

DUCDUNG NGUYEN (Graduate Student Member, IEEE) received the B.S. degree from the School of Electronics and Telecommunications, Vinh University, Nghe An, Vietnam, in 2018. He is currently pursuing the integrated M.S. and Ph.D. degree with the Department of Information Communication, Materials, and Chemistry Convergence Technology, Soongsil University, Seoul, South Korea. His current research interests include high-gain antenna, power amplifiers, metamaterials, wireless power transfer, and biomedical implantable antenna.

DANH MANH NGUYEN (Graduate Student Member, IEEE) received the B.Sc. (Eng.) degree in electronics and telecommunication from the School of Electronics and Telecommunication (SET), Hanoi University of Science and Technology, Hanoi, Vietnam, in 2020, and the M.S. degree from Soongsil University, Seoul, South Korea, in 2022, where he is currently pursuing the Ph.D. degree with the Department of Information Communication, Materials, and Chemistry Convergence Technology. His research interests include high gain antenna, wideband antennas, multiple-polarized antennas, wireless power transfer, and metamaterials.

CHULHUN SEO (Senior Member, IEEE) received the B.S., M.S., and Ph.D. degrees from Seoul National University, Seoul, South Korea, in 1983, 1985, and 1993, respectively. From 1993 to 1995, he was with the Massachusetts Institute of Technology (MIT), Cambridge, MA, USA, as a Technical Staff Member. From 1993 to 1997, he was with Soongsil University, Seoul, as an Assistant Professor. From 1999 to 2001, he was a Visiting Professor with MIT. From 1997 to 2004, he was an Associate Professor with Soongsil University, where he has been a Professor in electronic engineering, since 2004. He was the Chairman of the IEEE MTT Korea Chapter, from 2011 to 2014. He is the President of the Korean Institute of Electromagnetic Engineering and Science (KIEES) and the Dean of the Information and Telecommunications College, Soongsil University. He is the Director of the Wireless Power Transfer Research Center, supported by the Korean Government's Ministry of Trade, Industry and Energy, and the Metamaterials Research Center, supported by Basic Research Laboratories (BRL) through an NRF Grant funded by the MSIP, and the Center for Intelligent Biomedical Wireless Power Transfer, supported by the National Research Foundation of Korea (NRF) funded by the MSIP. His research interests include wireless technologies, RF power amplifiers, and wireless power transfer using metamaterials.